THE JOURNAL OF BIOLOGICAL CHEMISTRY VOL. 282, NO. 38, pp. 28014–28024, September 21, 2007

Single Molecule Kinetic Analysis of Actin Filament Capping

*POLYPHOSPHOINOSITIDES DO NOT DISSOCIATE CAPPING PROTEINS**[S]

Received for publication, June 27, 2007, and in revised form, July 19, 2007 Published, JBC Papers in Press, July 26, 2007, DOI 10.1074/jbc.M705287200

Jeffrey R. Kuhn[‡1] **and Thomas D. Pollard**[‡§¶2]

From the Departments of [‡]*Molecular, Cellular, and Developmental Biology,* [§]*Molecular Biophysics and Biochemistry, and* [¶]*Cell Biology, Yale University, New Haven, Connecticut 06520*

We investigated how heterodimeric capping proteins bind to and dissociate from the barbed ends of actin filaments by observing single muscle actin filaments by total internal reflection fluorescence microscopy. The barbed end rate constants for mouse capping protein (CP) association of 2.6×10^6 M^{-1} s^{-1} and dissociation of 0.0003 s^{-1} agree with published values measured in bulk assays. The polyphosphoinositides (PPIs), phosphatidylinositol 3,4-bisphosphate (PI(3,4)P_2), PI(4,5)P_2, and PI(3,4,5)P_3, prevent CP from binding to barbed ends, but three different assays showed that none of these lipids dissociate CP from filaments at concentrations that block CP binding to barbed ends. The affinity of fission yeast CP for barbed ends is a thousandfold less than mouse CP, because of a slower association rate constant (1.1×10^5 M^{-1} s^{-1}) and a faster dissociation rate constant (0.004 s^{-1}). PPIs do not inhibit binding of fission yeast CP to filament ends. Comparison of homology models revealed that fission yeast CP lacks a large patch of basic residues along the actin-binding surface on mouse CP. PPIs binding to this site might interfere sterically with capping, but this site would be inaccessible when CP is bound to the end of a filament.

The motility of animal cells depends on the coordinated assembly of actin filaments at the leading edge. Arp2/3 complex promotes actin polymerization by nucleating filaments that grow as branches from a mother filament (1, 2). Capping protein (CP,[3] called CapZ in muscle) appears to play an important role in generating the zone of short, highly branched actin filaments at the leading edge. CP is a heterodimer of structurally similar α and β subunits that form a mushroom-like structure with one flexible and one immobile COOH-terminal "tentacle" that bind the two terminal subunits of an actin filament (3). CP binds the barbed end of actin filaments tightly with a K_d of 0.1–1 nM. Given an association rate constant of 3–4 μM^{-1} s^{-1} and a cytoplasmic concentration of 1 μM (4), CP should terminate the growth of actin filaments with a half-time of about 0.2 s after their nucleation. Terminating growth quickly keeps the filaments short, so that they do not buckle under the force of polymerization as they push the membrane forward.

Vertebrate CP dissociates from barbed ends with a half-time of 30 min (4), far too slow for simple, spontaneous dissociation to be involved with the conversion of the network of short, branched filaments at the leading edge to longer, unbranched filaments toward the cell body. As CP prevents both dissociation of subunits from the barbed end and end-to-end filament annealing, some mechanism must accelerate the removal of CP from filament ends.

Both lipids and proteins, such as Ena/VASP (5–7) and CARMIL (8), can inhibit the interaction of CP with actin filaments. Polyphosphatidylinositides (PPIs) bind CP and block its interaction with filaments both *in vivo* (9) and *in vitro* (10). Addition of PIP_2 to mixtures of capped filaments, CP, and actin monomers *in vitro* increases the rate of polymerization (4). These experiments led to the widely accepted view that PPIs not only inhibit association of CP with barbed ends but also dissociate CP from actin filaments. These two effects are postulated to bias the growth of actin filament branches toward the inside of the plasma membrane at the leading edge (11, 12). Steric interference would be the simplest way for PPIs to block interaction of CP with filament ends. Mutation of three residues surrounding a putative PIP_2-binding site reduces the affinity of CP for PIP_2 5–60-fold and barbed ends 400-fold (13). Although the binding sites on CP for the barbed end and PIP_2 overlap, dissociation of CP from a barbed end by PIP_2 would presumably require an allosteric mechanism.

To examine the question of uncapping from a new perspective, we used total internal reflection fluorescence (TIRF) microscopy to observe capping and uncapping of individual filaments *in vitro*. We obtained association and dissociation rate constants for vertebrate CP in good agreement with those previously measured in bulk assays. We also confirmed that PI(3,4)P_2, PI(4,5)P_2, and PI(3,4,5)P_2 sequester CP and prevent its binding to barbed ends. However, none of these PPIs accelerated the dissociation of CP from filaments. Although PIP_2 inhibits budding yeast CP (14), we discovered that PPIs do not inhibit binding of fission yeast CP to filament ends, despite other similarities to budding yeast and vertebrate CPs. This experiment of nature gave us an opportunity to identify an excellent candidate for an alternate PPI-binding site by com-

* This work was supported by National Institutes of Health Research Grant GM-26338 (to T. D. P.) and a Burroughs Wellcome Fund Career Award at the Scientific Interface (to J. R. K.). The costs of publication of this article were defrayed in part by the payment of page charges. This article must therefore be hereby marked "*advertisement*" in accordance with 18 U.S.C. Section 1734 solely to indicate this fact.

[S] The on-line version of this article (available at http://www.jbc.org) contains supplemental Fig. 1.

[1] Present address: Dept. of Biology, Virginia Polytechnic Institute and State University, Blacksburg, VA 24061-0406.

[2] To whom correspondence should be addressed: MCDB, KBT-548, Yale University, P.O. Box 208103, New Haven, CT 06520-8103. Fax: 203-432-6161; E-mail: thomas.pollard@yale.edu.

[3] The abbreviations used are: CP, capping protein; TIRF, total internal reflection fluorescence; PPI, polyphosphoinositide; PI, phosphatidylinositol; PIP_2, phosphatidylinositol 4,5-bisphosphate; OG, Oregon Green 488; *Mm*CP, *Mus musculus* CP; *Sp*CP, *S. pombe* CP; HMM, hidden Markov model; MIL, maximum interval likelihood; ddH_2O, double distilled H_2O.

paring the electrostatic surface potentials of homology models of CPs that differ in their ability to bind PPIs.

EXPERIMENTAL PROCEDURES

Proteins

We purified actin from rabbit skeletal muscle acetone powder through one round of polymerization, depolymerization, and gel filtration (15). Actin was labeled with pyrenyl iodoacetamide (Molecular Probes, Eugene, OR) (16) or with Oregon Green 488 (OG) iodoacetamide (Molecular Probes, Eugene, OR) and further purified with DEAE-Sepharose ion exchange chromatography followed by depolymerization and gel filtration (15). Before use, labeled and unlabeled actins were dialyzed overnight against fresh buffer G (2 mM Tris-Cl, pH 8, 0.2 mM ATP, 1 mM NaN_3, 0.1 mM $CaCl_2$, 0.5 mM dithiothreitol (DTT)) and centrifuged at 100,000 × *g* for 2 h at 4 °C.

Recombinant mouse capping protein (*Mm*CP) α1 and β2 subunits were expressed on a single plasmid (pET3d[m-α1/β2]) and purified from bacterial lysates (17). We purified recombinant fission yeast capping protein (*Sp*CP) subunits Acap1 and Acap2 expressed on a single plasmid (pET3a-acp1acp2) (18). Capping proteins were dialyzed into Ca^{2+}/Mg^{2+}-free CP buffer (10 mM imidazole, pH 7.5, 50 mM KCl, 1 mM DTT, 0.1 mM EGTA, 2 mM NaN_3) containing 50% glycerol, flash-frozen in liquid N_2, and stored at −80 °C. We determined the activity of a frozen *Mm*CP stock by equilibrating a range of *Mm*CP concentrations with actin seeds and then measuring the rate of pyrene actin assembly from capped seeds (10). Frozen stocks were 2–4-fold less active than freshly prepared *Mm*CP. Myosin from rabbit skeletal muscle (19) was treated with *N*-ethylmaleimide (Sigma) (20) and stored at −20 °C in 10 mM imidazole, pH 7, 0.5 M KCl, 1 mM DTT, and 50% glycerol.

We estimated protein concentrations from the following extinction coefficients: unlabeled actin, A_{290} = 26,600 M^{-1} cm^{-1} (21); *Mm*CP, A_{280} = 76,300 M^{-1} cm^{-1} (17); *Sp*CP, A_{280} = 72,000 M^{-1} cm^{-1} (18); myosin, A_{280} = 260,000 M^{-1} cm^{-1} (22). For OG-labeled actin, total actin concentration was estimated from the corrected extinction coefficient, $A_{290} - 0.17 \times A_{491} = A^*_{290}$ = 26,600 M^{-1} cm^{-1}, and labeled actin fraction from A_{491} = 77,800 M^{-1} cm^{-1} (15). For pyrene-labeled actin, total actin concentration was estimated from the corrected extinction coefficient, $A_{290} - 0.127 \times A_{344} = A^*_{290}$ = 26,600 M^{-1} cm^{-1} and labeled actin fraction from A_{344} = 22,000 M^{-1} cm^{-1} (23).

Synthetic D-myo-phosphatidylinositols (diC16) from Echelon Biosciences (Salt Lake City, UT) were resuspended in chloroform, aliquoted into glass vials, dried under vacuum or nitrogen gas, and stored at −20 °C. Before use, we added Ca^{2+}/Mg^{2+}-free CP buffer to an aliquot of phospholipid to a final concentration of 200 μM, incubated at 4 °C for 4–16 h to suspend, and sonicated for 5 min in a water bath sonicator and an additional 1 min before each experiment to form micelles.

TIRF Polymerization Experiments

Crown glass slides were cleaned and prepared as flow cells (15). We preincubated each flow cell for 2 min with 0.2 μM *N*-ethylmaleimide-inactivated myosin in high salt Tris-buffered saline (50 mM Tris-Cl, pH 7.6, 600 mM NaCl) containing a 10^{-4} dilution of 200 nm crimson fluorescent microspheres (Molecular Probes, Eugene, OR) followed for 1 min each with 1% bovine serum albumin (Sigma) in high salt Tris-buffered saline and then 1% *N*-ethylmaleimide in low salt Tris-buffered saline (50 mM Tris-Cl, pH 7.6, 150 mM NaCl).

We mixed labeled and unlabeled Ca-ATP-actin to the desired labeled fraction at 4.44× the final concentration, mixed 9:1 with 10× Mg exchange buffer (10× ME: 10 mM EGTA, 1 mM $MgCl_2$), and incubated on ice for 2 min to form 4× final concentration of Mg-ATP actin. We placed 8 μl of Mg-ATP at the bottom of a 1.5-ml Eppendorf tube, and on the side, we mixed 4 μl of 8× final concentrations of Ca^{2+}/Mg^{2+}-free CP or buffer and 4 μl of 8× final concentrations of phospholipid or buffer and incubated at room temperature for 5 min. To start the reaction, we washed both drops together with 16 μl of 2× TIR buffer (2×: 100 mM KCl, 2 mM $MgCl_2$, 2 mM EGTA, 20 mM imidazole, pH 7.0, 200 mM DTT, 0.4 mM ATP, 30 mM glucose, 1% methylcellulose, 40 μg/ml catalase, 200 μg/ml glucose oxidase) and wicked 16 μl through a prepared flow chamber. All subsequent buffer exchanges were similar except that Mg-buffer G (9:1 mixture of buffer G, 10× ME) was substituted for Mg-ATP-actin when pre-existing filaments were incubated with CP alone before dissociation experiments. For longer uncapping experiments, we sealed the chamber ends with VALAP (1:1:1 Vaseline/lanolin/paraffin) to reduce filament breakage because of evaporative loss induced flow. Images were captured once every 6–60 s, depending on conditions, for a total of 100–200 frames per experiment.

Bulk Pyrenyl-Actin Spectroscopy Assay of Growth from Capped Seeds

Long Seeds—We mixed Ca-ATP-actin 8:1 with 10× ME and incubated on ice for 2 min followed by 9:1 mix with 10× KMEI (10×: 500 mM KCl, 10 mM $MgCl_2$, 10 mM EGTA, 100 mM imidazole, pH 7) for a final Mg-ATP-actin concentration of 6 μM. Filaments were polymerized at 20 °C for over 2 h and used without dilution.

Short Seeds—6 μM Mg-ATP-actin was mixed as above, polymerized for 10 min, diluted 1:9 in buffer F (8:1:1 mixture of buffer G, 10× ME, 10× KMEI), and vortexed for 10 s on maximum speed (Vortex Genie 2, VWR Scientific Products, West Chester, PA). We used short seeds 1 min after vortexing. Average seed length was calculated from [filament]/[ends] after dilution.

Capped Seeds—We gently added undiluted long seeds or freshly prepared short seeds 1:1 to a drop of 150 nM *Mm*CP and incubated for 5 min. Wide-bore pipette tips (USA Scientific, Ocala, FL) and gentle pipetting were used in all subsequent mixing steps.

Elongation from Capped Seeds—2.5 μM (30% pyrenyl) Ca-ATP-actin monomers were converted to Mg-ATP-actin by mixing 10:1 with 10× ME on ice for 2 min. Separate drops of capped seeds, pyrenyl-actin, and PPI were mixed together with buffer F for a final 15-fold dilution of seeds and a final concentration of 10 nM *Mm*CP, 1.2 μM (30% pyrenyl), Mg-ATP-actin, and 24 μM PPI. A Gemini XPS fluorescence microplate reader (Molecular Devices, Sunnyvale, CA) monitored the fluorescence increase over time with excitation at 365 nm and emission at 407 nm.

Calculation of [Filamentous Actin] and [Ends]—Scatter from PPI micelles increased the fluorescent signal by a constant amount (4). Assuming that the concentration of filamentous pyrenyl-actin was zero at the beginning of the reaction and the polymerization rate was constant for the first 4 min, we used a linear fit of the first 250 s of each polymerization trace to estimate fluorescence intensity at 0 s and subtracted this value. Seeded actin polymerization curves that reached a plateau were used to estimate the final fluorescence intensity for [filament] = 1.2 − 0.17 = 1.03 μM, assuming a critical concentration of K_C = 0.17 μM, and for [actin] = 1.2 − [filament]. We applied these scaling factors to all curves and obtained polymerization rates from the slope of a 250-s window of data. Using polymerization rate constants of k_+ = 12.9 $\mu M^{-1}\ s^{-1}$ and k_- = 2.2 s^{-1} (24), we estimated the concentration of ends as [ends] = rate/(12.9[actin] − 2.2).

Bulk Rhodamine-Phalloidin Fixation of Filaments Grown from Capped Seeds

Avidin-coated Coverslips—Coverslips were cleaned for 30 min with a 1:9 mixture of H_2O-saturated KOH/ethanol, rinsed thoroughly with ddH_2O, cleaned for 30 min in 2 M HCl, and rinsed with ddH_2O. Coverslips were coated with 5% γ-aminopropyltriethoxy-silane (Aldrich) in 95% ethanol, 5% H_2O, pH 5, with acetic acid, for 1 h and rinsed thoroughly with ethanol. Coverslips were dried with N_2 gas, coated for 1 h with avidin (Sigma), dissolved to 1 mg/ml in 10 mM Tris, pH 8, 2.5% ethanol, rinsed in ddH_2O, and dried with N_2 gas (25).

Marked Capped Seeds—We converted 60% OG-labeled Ca-ATP-actin monomers to 2 μM Mg-ATP-actin by mixing 9:1 with 10× ME on ice for 2 min. Short seeds (see above) were diluted an additional 2-fold before mixing 1:1 with 60% OG Mg-ATP-actin monomers for 1 min to mark barbed ends. We then mixed the products 2:1 with 60 nM *Mm*CP for 5 min to cap barbed ends.

Marked Elongation from Capped Seeds—20% OG Ca-ATP-actin monomers were mixed 9:1 to a final concentration of 8 μM with 1× ME on ice for 2 min. To 25 μl of 2× buffer F, we added 5 μl of 8 μM (20% OG) actin monomers and 5 μl of 200 μM PPI. 15 μl of capped seeds were slowly added using a large orifice tip, and the reaction was incubated for 5 min before the addition of 5 μl of 10 μM (40% rhodamine-, 60% biotin-labeled) phalloidin to label and stabilize filaments. After 5 min, stabilized filaments were slowly diluted 20–40-fold in 1× TIR buffer, and 6 μl was added to a slide and covered with an avidin-coated coverslip.

Data Collection and Analysis

We modified an Olympus (Melville, NY) IX-71 microscope for prism-based TIRF microscopy (15). We captured and processed all images with custom-designed Java plug-ins for ImageJ (National Institutes of Health, rsb.info.nih.gov). Crimson fluorescent beads at the slide surface acted as autofocus targets (15).

We traced filaments and created linear kymographs using a custom plug-in for ImageJ (15). A maximum intensity search algorithm "snapped" a rough hand trace to the filament center to create a refined filament trace and measure total length. For linear kymographs, the plug-in sub-sampled filament intensities at 1 pixel increments along this refined trace and past both ends and replotted intensities as a single column with horizontal position dictated by frame number. We collected length measurements for each filament over several frames and analyzed growth in a standard Excel (Microsoft Corp., Redmond, WA) spreadsheet. Filament length was converted to subunits using 370 subunits/μm (26).

To measure CP association times, we added CP to pre-existing filaments concomitantly with a higher labeled fraction of actin. Once the barbed end growth of a filament was halted, we measured the length from the jump in filament brightness to the end of the filament through several frames. The average of this length, $\bar{L}_t$, divided by the separately measured linear growth rate, R, gave the time between addition and capping, $t_c = \bar{L}_t/R$. To measure CP dissociation rates, we washed CP from pre-existing filaments with 2 chamber volumes of buffer concomitantly with a higher labeled fraction of actin. Upon barbed end growth resumption, we traced length of the bright filament segment through several frames and estimated the uncapping time, t_u, from the average measured time and length and the separately measured growth rate as $t_u = \bar{t} - \bar{L}_t/R$.

We estimated the affinity of *Mm*CP for PPI from the decrease in the apparent association rate constant in the presence of PPI. Assuming that PPI binding decreased available CP by mass action, the ratio of available to total CP, $r = [C_{avail}]/[C_{total}]$, was determined from the decrease in the apparent association rate in PPI compared with the native association rate, k_+, as $r = k_{+,app,PPI}/k_+$. The affinity of CP for PI was estimated from $K_{d,PPI} = [C_{avail}] \times [PPI]/[C{\cdot}PPI]$, or $K_{d,PPI} = r \times [PPI]/(1 - r)$.

For hidden Markov modeling (HMM) of *Sp*CP association/dissociation, we measured lengths of 10–15 filaments per experiment through every frame. A Savitzky-Golay smoothing derivate filter (27) transformed each length trace L_i into smoothed instantaneous growth rates at each time point. These instantaneous growth rates were uniformly high during obvious uncapped states and near zero during capped states. With these instantaneous growth rates as reporters of the true hidden barbed-end state (capped or uncapped), we used QuB kinetic analysis software, available on line (28, 29), for Baum-Welch idealization and to estimate rate constants for capping and uncapping. We assumed a simple, second-order model for capping protein (C) binding to Mg-ATP-actin filament barbed ends (A_n) of

$$A_n + C \leftrightarrow A_nC$$

REACTION 1

Maximum interval likelihood (MIL) analysis of the frequency of durations of all capped or uncapped states yielded a rate, k_1, for the transition from an uncapped to a capped state, and a transition rate constant, k_2, for the reverse. At high CP concentrations, the durations of uncapped states decreased toward the acquisition frequency and were more likely to be hidden, increasing error in the estimation of k_2. At low CP concentrations, the frequency of capping and subsequent uncapping events decreased, increasing error in both k_1 and k_2. For comparison across all concentrations, we summed the two transition rates to form a single apparent equilibrium rate ($k_{app} = k_1 + k_2$),

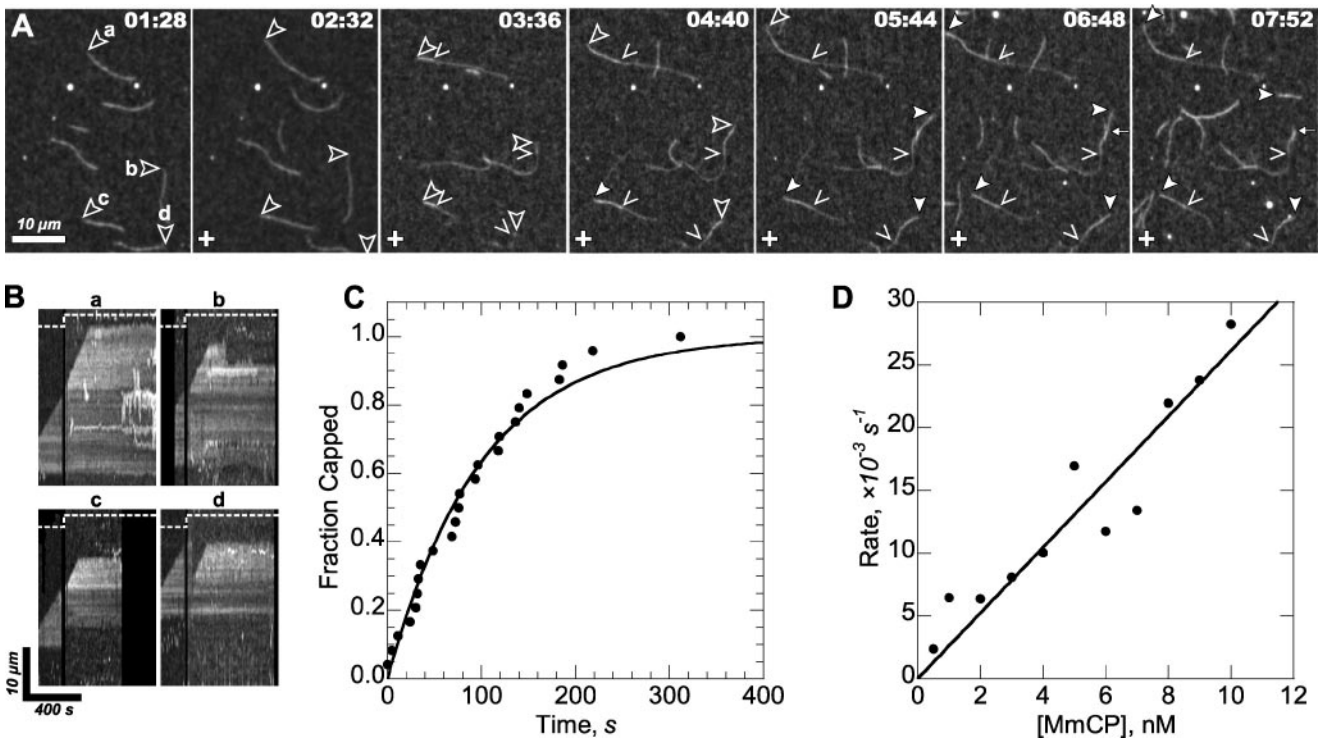

FIGURE 1. **Association of murine CP with the barbed ends of growing actin filaments.** Conditions used were as follows: 2 μM (20 or 40% Oregon Green 488-labeled) Mg-ATP actin, 0–10 nM *Mm*CP, 10 mM imidazole, pH 7.0, 50 mM KCl, 1 mM $MgCl_2$, 1 mM EGTA, 100 mM DTT, 0.2 mM ATP, 50 μM $CaCl_2$, 15 mM glucose, 20 μg/ml catalase, 100 μg/ml glucose oxidase, 0.5% methylcellulose at 25 °C. *A–C,* filaments grown in 4 nM *Mm*CP. *A,* time course of filament growth. Initially 20% labeled Mg-ATP-actin was polymerized, and growing filament barbed ends (*open arrowheads*) were observed by TIRF microscopy. The buffer was exchanged with 40% labeled Mg-ATP-actin and 4 nM *Mm*CP (*plus symbols*). *Wedges* mark the transition to brighter filament sections growing in the presence of *Mm*CP. *Filled arrowheads* mark the times when individual barbed ends ceased growth. Numbers (*min/s*) indicate frame times. *Scale bar* is 10 μm. *B,* linear kymographs of individual filaments *a–d* from *A* with time on the *horizontal axis* and length on the *vertical axis*. Filament barbed ends are oriented at top. The steps in the *dashed lines* indicate when *Mm*CP was added. *C,* time course of capping of 24 filaments in 4 nM *Mm*CP (●). An exponential fit (*line*) gave k_{obs} of 0.01 s^{-1}. *D,* dependence of k_{obs} on the concentration of *Mm*CP (322 total events). The slope gave an association rate constant of 2.6 ± 0.1 $\times 10^6$ M^{-1} s^{-1}.

similar to the rate for a bulk assay to reach equilibrium. This apparent rate was less sensitive to concentration-dependent error than the either transition rate alone. The association and dissociation rate constants, k_+ and k_-, were obtained either from the slope and *y* intercept of the apparent rate *versus* concentration or in single [CP] experiments from an average over three experiments as $k_+ = k_1/[CP]$ and $k_- = k_2$.

Homology Modeling

We aligned multiple CP sequences using the MUSCLE algorithm (30) and submitted aligned sequences to Swiss-Model (31) for construction and refinement of homology models based on the structure of chicken $\alpha1\beta1$ CapZ, Protein Data Bank code 1IZN (3). We calculated electrostatic surface potentials with the Adaptive Poisson-Boltzmann Solver (APBS) Package (32) at pH 7 and 50 mM ion concentration. Molecular surfaces were calculated and displayed using University of California, San Francisco, Chimera (33) and colored for iso-potential values of −15, 0, and +15 k_BT/e_c.

RESULTS

Kinetics of Capping and Capping by Mouse Capping Protein—We observed the growth and capping of individual actin filaments by TIRF microscopy using muscle actin-labeled with Oregon Green (OG-actin). For example, Fig. 1*A* shows a time course of filaments polymerizing in 2 μM Mg-ATP-actin monomer before and after the addition of 4 nM murine capping protein (*Mm*CP) to the reaction buffer. Straightened kymographs of individual filaments (Fig. 1*B*) show linear barbed-end growth that was terminated by capping protein. The fraction of capped filaments in a sample followed an exponential time course, consistent with pseudo first-order conditions (Fig. 1*C*). As slow mixing occasionally caused a lag in capping during the 1st min of observation, we discarded the first few capping events in these experiments to maximize the "goodness of fit" to an exponential (R^2 value). The exponential association rate depended linearly on *Mm*CP concentration over a 20-fold range (Fig. 1*D*), giving an association rate constant of 2.6 ± 0.1 μM^{-1} s^{-1} for *Mm*CP binding to Mg-ATP-actin filament barbed ends (Table 1). This value is similar to previous measurements in bulk samples of 3.5 μM^{-1} s^{-1} for purified chicken CP $\alpha1\beta1$ (4) and 6.3 μM^{-1} s^{-1} for recombinant chicken CP $\alpha1\beta1$ (34). Occasionally in experiments

TABLE 1
Mouse Capping protein rate and equilibrium constants

Experiment	k_+	k_-	$K_{d,BE}$
	$\times 10^6$ $M^{-1}\cdot s^{-1}$	$\times 10^{-4}$ s^{-1}	nM
Control	2.6 ± 0.1	2.7 ± 0.1	0.10
1 mM Mg^{2+}, PI buffer	2.6 ± 0.2	2.2 ± 0.1	0.08
0.1 mM Mg^{2+}, PI buffer	2.6 ± 0.3	3.1 ± 0.2	0.12
Chicken CP, Schafer *et al.* (4)	3.5	4	0.08

[a] Dissociation of CP from filament barbed ends, estimated from k_-/k_+.

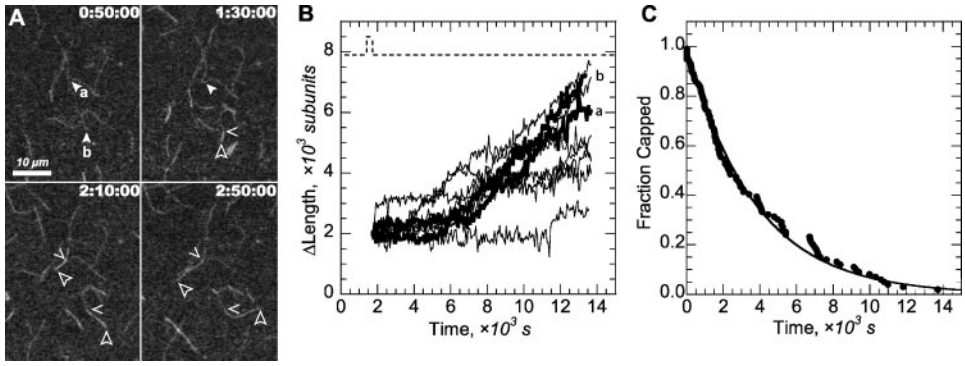

FIGURE 2. **Dissociation of murine CP from filament barbed ends.** Conditions used were as follows: buffers as in Fig. 1. *A,* time course of filament elongation observed by TIRF microscopy. Initially 2 μM (25% labeled) Mg-ATP-actin was polymerized in a flow cell for 6–8 min (not shown) and exchanged with a solution of 20 nM *Mm*CP without free actin for 5 min (22× association half-times), followed by a solution of 0.4 μM (50% labeled) Mg-ATP-actin without capping protein and observed for 3 h at 1-min intervals. Capped filament barbed ends (*closed arrowheads*) grew as brighter segments upon CP dissociation (*wedge* to *open arrowhead*). Representative filaments marked *a* and *b* are highlighted in *B* (*bold lines*). Numbers (*min/s*) indicate frame times. *Scale bar* is 10 μm. *B,* time course of actin filament lengths after the transient pulse of 20 nM *Mm*CP (*dashed line*). *C,* time course of uncapping of all 99 filaments observed in three experiments (●). An exponential fit (*line*) gave a dissociation rate constant of 2.7 ± 0.1 $\times 10^{-4}$ s^{-1}.

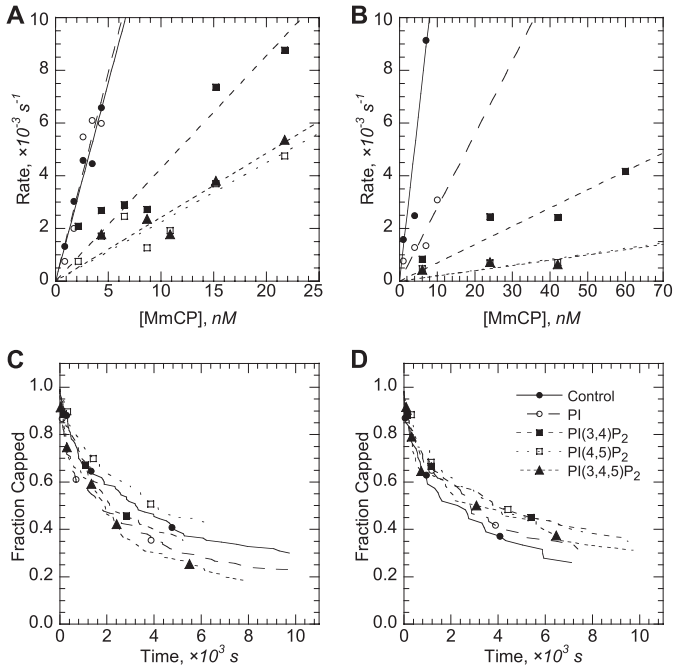

FIGURE 3. **Effects of phosphoinositides on association and dissociation of *Mm*CP on filament barbed ends in high and low concentrations of Mg^{2+}.** Conditions used were as follows: general buffers as in Fig. 1; the buffer in *A* and *C* contained 1 mM $MgCl_2$, 1 mM EGTA; the buffer in *B* and *D* contained 0.1 mM $MgCl_2$, 1 mM EGTA. Symbols are defined in *D*. *A* and *B,* dependence of the observed rate of capping on the concentration of *Mm*CP in the presence of 25 μM phosphoinositides. Filaments were polymerized from 1 μM (25% labeled) Mg-ATP-actin for 5–10 min in a flow cell. Capping was initiated by exchanging the flow cell buffer with a solution containing 0.5 μM (50% labeled) ATP-actin and a range of concentrations of *Mm*CP preincubated in Ca^{2+}/Mg^{2+}-free buffer with 25 μM phosphoinositide for 5 min. We analyzed the time courses of ~190 capping events (total of all *Mm*CP concentrations) per PPI condition (*A*) or 120 total capping events per PPI condition (*B*) as in Fig. 1 to obtain association rates at each concentration of *Mm*CP. *C* and *D,* time course of uncapping filaments in the presence of 25 μM phosphoinositides. Filaments were grown in flow cells from 1 μM (25% labeled) Mg-ATP-actin for 5–10 min and capped by exchanging with buffer containing 20 nM *Mm*CP without free actin for 5 min. Uncapping was initiated by exchanging the buffer with 0.25 μM (50% labeled) Mg-ATP-actin and 25 μM of the indicated phosphoinositide or buffer. We analyzed an average of 74 *Mm*CP dissociation events (*C*) or 50 dissociation events (*D*) from three different experiments per condition as in Fig. 2 to obtain dissociation rate constants.

without capping protein, one or two growth pauses occurred during observation of a field containing many filaments because of surface binding effects. The rarity of these events precluded analysis of this pseudo-capping.

Murine capping protein dissociated slowly from filament barbed ends when we washed out free CP (Fig. 2*A*). We interpret the onset of growth as dissociation of *Mm*CP. Most filaments grew at a constant rate (Fig. 2*B*), but a few were re-capped and stopped elongating. The fraction of capped filaments declined exponentially over time (Fig. 2*C*), giving a dissociation rate constant of 2.7 ± 0.1 $\times 10^{-4}$ s^{-1} (half-time of 43 min). The ratio of the dissociation and association rate constants gave a K_d of 103 ± 7 pM (Table 1), similar to previous measurements with bulk samples of 80 pM for chicken capping protein (4, 34).

Effects of Polyphosphoinositides on Capping and Uncapping by Mouse Capping Proteins—Polyphosphoinositides bind capping proteins and inhibit capping of barbed ends in bulk samples (10). Our observations of individual actin filaments confirmed that 25 μM concentrations of micelles of three different PPIs inhibit the rate of capping over a range of capping protein concentrations (Fig. 3*A*; Table 2). The dependence of the capping rate on *Mm*CP concentration was the same in controls and with 25 μM PI, but it was 3.5-fold lower in $PI(3,4)P_2$, 6.7-fold lower in $PI(4,5)P_2$, and 6.2-fold lower in $PI(3,4,5)P_3$. Assuming that *Mm*CP bound to micelles cannot bind filaments and that these rates were lower because of mass action, *Mm*CP would have dissociation equilibrium constants for PPIs of 4.4 to 10 μM (Table 2).

Divalent cations such as Mg^{2+} are thought to inhibit PPI binding to CP either through micelle aggregation (35) or charge masking. At low $MgCl_2$ concentrations (0.1 mM), the association of CP with barbed ends (Fig. 3*B*; Table 2) was 10-fold slower in $PI(4,5)P_2$ and $PI(3,4,5)P_3$ than at high $MgCl_2$ concentrations and 5-fold slower in $PI(3,4)P_2$. Lowering Mg^{2+} concentrations increased the apparent affinity of CP for PPIs to 0.4–1.5 μM. CP association with filaments was also slower in PI than in buffer under low Mg^{2+} conditions, indicating that the phosphate linking the inositol ring to the lipid moiety may play some role in PPI binding.

We used bulk samples to evaluate the concentration of barbed ends available for elongation by pyrenyl actin in 0.1 mM Mg^{2+}. Under conditions where the polymerization rate depended on the concentration of ends, we confirmed (Fig. 4*A*) that addition of PIP_2 to bulk samples of capped actin filaments increased the concentration of ends (10, 36). Polymerization was faster in PIP_2 and PIP_3 than in PI or control capped filaments (Fig. 4*A*). The most straightforward interpretation of the high elongation rates is that PIP_2 and PIP_3 promote dissociation of capping protein from barbed ends. However, dissociation

TABLE 2
Mouse capping protein association and dissociation rates with PPIs

Experiment	$k_{+,app}$ [a]	$k_{-,app}$ [a]	$K_{d,PPI}$ [b]
	$\times 10^6\ M^{-1}\cdot s^{-1}$	$\times 10^{-4}\ s^{-1}$	μM
1 mM Mg^{2+}, 25 μM PI	2.7 ± 0.3	3.4 ± 0.2	
1 mM Mg^{2+}, 25 μM PI(3,4)P_2	0.74 ± 0.05	3.0 ± 0.1	9.9
1 mM Mg^{2+}, 25 μM PI(4,5)P_2	0.39 ± 0.04	1.9 ± 0.1	4.4
1 mM Mg^{2+}, 25 μM PI(3,4,5)P_3	0.42 ± 0.03	3.7 ± 0.2	4.8
0.1 mM Mg^{2+}, 25 μM PI	0.58 ± 0.08	2.4 ± 0.1	7.1
0.1 mM Mg^{2+}, 25 μM PI(3,4)P_2	0.15 ± 0.02	1.8 ± 0.1	1.5
0.1 mM Mg^{2+}, 25 μM PI(4,5)P_2	0.04 ± 0.01	1.9 ± 0.1	0.42
0.1 mM Mg^{2+}, 25 μM PI(3,4,5)P_3	0.04 ± 0.01	2.1 ± 0.2	0.40

[a] Apparent association and dissociation rates are shown.
[b] Dissociation of CP from polyphosphoinositide was estimated from the decrease in $k_{+,app}$ by mass action (see "Experimental Procedures").

would have to be fast, given the absence of a lag after adding the PPIs to capped filaments in both the published work and in our experiments. In contrast, none of the PPIs uncapped filaments in the microscopic assay (Fig. 3, *C* and *D*). Neither PI, PI(3,4)P_2, PI(4,5)P_2, nor PI(3,4,5)P_3 significantly altered the time course of *Mm*CP dissociation in either 0.1 or 1.0 mM Mg^{2+} in these microscopic assays.

Given this difference between the bulk and microscopic assays, we considered the possibility that filaments break during mixing bulk samples and that PPIs prevent recapping by sequestering free CP. Although we mixed capped seeds with PPIs in bulk experiments slowly and with large orifice pipette tips, any shearing force would potentially break filaments of moderate length or entangled in a network (37).

To test this hypothesis we compared the effect of PPIs on elongation of long and short capped seeds diluted to a similar concentration of ends (Fig. 4, *A* and *B*). The mean length of long seeds was 21 μm based on the rate of elongation measured with pyrene actin in bulk samples (Fig. 4*E*). These long filaments tended to be entangled in bundles typically longer than 10 μm when viewed by fluorescence microscopy (Fig. 4*F*). The free filaments in these samples measured 7 ± 7 μm long (Fig. 4*F*). The mean length of the short filament seeds made by vortexing polymerized actin was 1.6 ± 1.4 μm by microscopy (Fig. 4*G*) and 2.7 μm by the elongation assay (Fig. 4*E*).

We used elongation experiments with 1.2 μM pyrenyl actin monomers (Fig. 4, *C* and *D*) to measure the concentrations of uncapped barbed ends over time (Fig. 4, *C–E*). Mouse capping protein reduced the rate of elongation of both long and short seeds and thus the concentrations of free ends 10-fold. Mixing 25 μM PI with either long or short capped seeds had no effect on the rate of elongation. Mixing long capped seeds with PPIs increased the elongation rate (Fig. 4*A*) and thus the concentration of free barbed ends (Fig. 4*E*). These increases were 6-fold by PI(3,4)P_2, 6-fold by PI(4,5)P_2, and 4-fold by PI(3,4,5)P_3, a significant portion of the 8-fold difference in free ends between uncapped and capped long seeds. In contrast, mixing short capped seeds with PI(3,4)P_2, PI(4,5)P_2, or PI(3,4,5)P_3 increased the elongation rate only 1.4–2.8-fold (Fig. 4*D*), a small fraction of the average 11-fold difference in free ends between uncapped and capped short seeds. As these experiments were done side-by-side, we conclude that longer, entangled seeds are more likely to break during mixing than short seeds, and that much generation of free barbed ends is because of filament breakage and sequestration of CP by PPIs rather than uncapping. Because the results in bulk polymerization assays were similar in buffers containing 0.1 and 1.0 mM Mg^{2+} (not shown) and because the Mg^{2+} concentration did not affect uncapping in microscopic assays, we performed all subsequent experiments at 1 mM $MgCl_2$ concentrations.

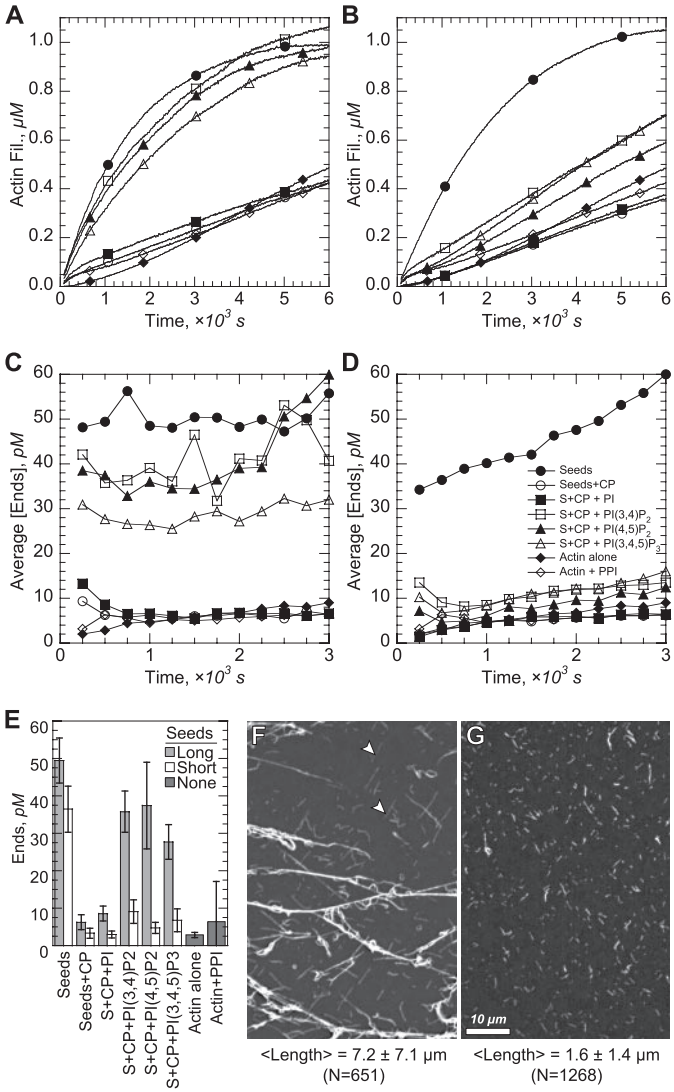

FIGURE 4. **Influence of seed length on PPI-mediated "uncapping" of filaments.** Conditions used were as follows: 1.2 μM (30% pyrene labeled) Mg-ATP actin, 10 nM final *Mm*CP, 25 μM PPI in polymerization buffer (10 mM imidazole, pH 7.0, 50 mM KCl, 0.1 mM $MgCl_2$, 1 mM EGTA, 0.5 mM DTT, 0.2 mM ATP, 0.1 mM $CaCl_2$) at 25 °C. *A–D,* effect of *Mm*CP and PPIs on the time course of elongation of actin filament from seeds measured by the fluorescence of pyrene-labeled actin. Curves are averages from at least three experiments. Symbols marking fluorescent traces are defined in *D*. *A,* elongation from long seeds alone or long seeds preincubated with 75 nM *Mm*CP and further diluted in polymerization buffer with pyrene actin with or without 25 μM of various PPIs. Long seeds were assembled from 6 μM Mg-ATP-actin over 2 h. *B,* elongation from short seeds in the same conditions as *A*. Short seeds were prepared immediately before use by polymerizing 6 μM Mg-ATP-actin for 10 min, diluting 10-fold into polymerization buffer, and shearing on a lab vortex mixer for 10 s. *C* and *D,* concentration of filament ends over time calculated from *A* and *B*. End concentrations shown for long seeds (*C*) or short seeds (*D*) are an average of three experiments. *E,* concentration of ends at 500 s for long (*gray bars*) and short (*white bars*) seeds. Values shown are the average and S.D. of three experiments. *F,* fluorescence micrograph of long seeds stained with rhodamine-phalloidin. Lengths of entangled filaments could not be measured, but the average length of isolated filaments (*arrowheads*) is indicated below (mean ± S.D.). Entangled filament bundles were typically much longer than 10 μm. *G,* fluorescence micrograph of short seeds. Staining with rhodamine-phalloidin showed that these seeds were short (1.6 μm) and not entangled. *Scale bar* is 10 μm.

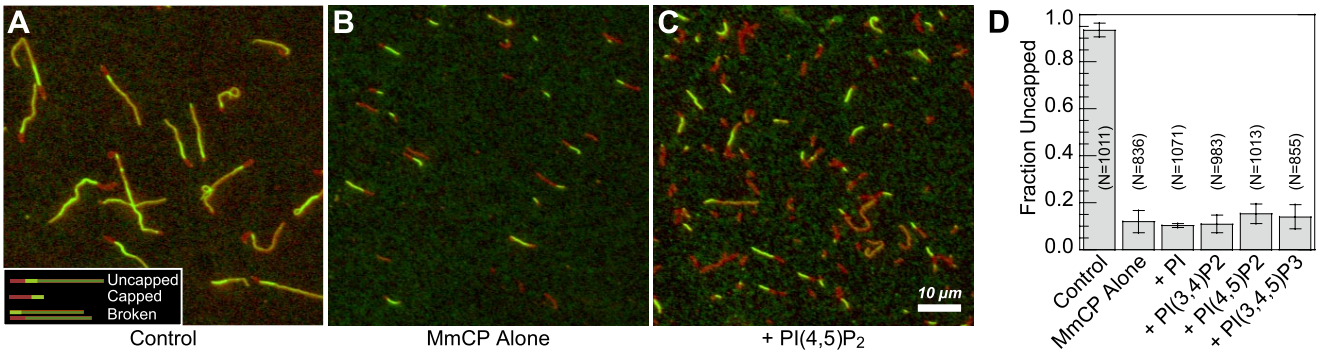

FIGURE 5. **Alternative microscopic assay to evaluate uncapping by phosphoinositides.** Conditions used were as follows: buffers as in Fig. 4 except 1 mM $MgCl_2$ and 1 mM EGTA. *A–C,* fluorescence micrographs of actin filaments. Short unlabeled actin seeds were incubated for 1 min in 1 μM, 60% Oregon Green-labeled Mg-ATP-actin followed by reaction with 20 nM *Mm*CP for 5 min in 60% Oregon Green-labeled actin diluted to 0.7 μM. Capped seeds were diluted in 1 μM, 20% Oregon Green-labeled Mg-ATP-actin and Ca^{2+}/Mg^{2+} free PPI to a final concentration of 6 nM *Mm*CP and 20 μM PPI, polymerized for 5 min, and stained with rhodamine-phalloidin (40% labeled). *A,* elongation of marked filaments prepared without *Mm*CP or PPI showing uncapped filaments (see *inset*). *B,* incubation of marked filaments capped with *Mm*CP and followed with actin monomers without PPI showing no barbed end growth (see *inset* in *A*). *C,* capped filaments incubated with $PI(4,5)P_2$ for 5 min showing mostly capped filaments and a few filaments that elongated from broken ends. *Scale bar* is 10 μm. *D, bar chart* of the fraction of uncapped filaments, excluding broken filaments (average and S.D. of three experiments). *N* is the number of filaments scored for each condition.

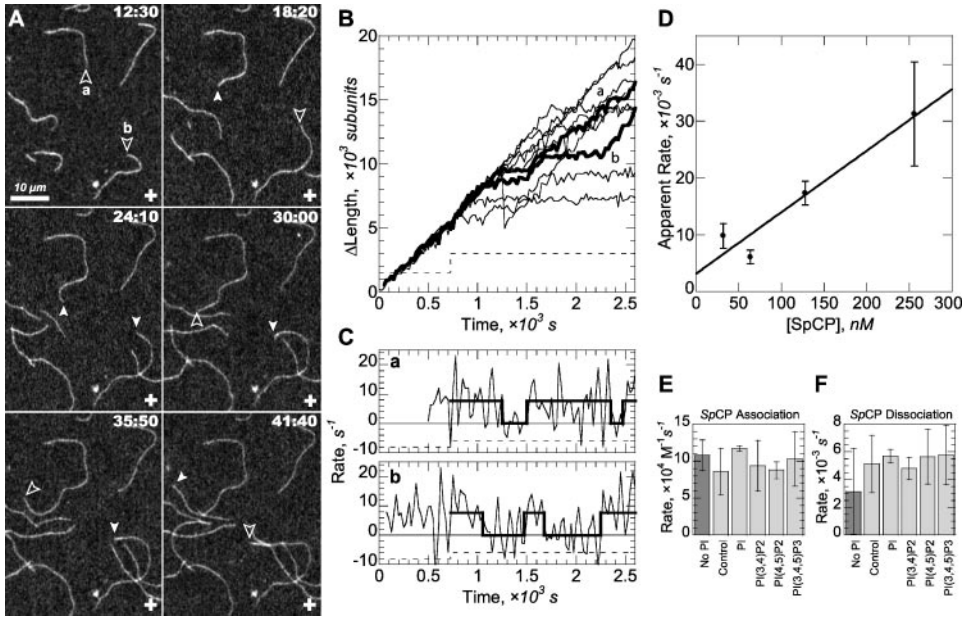

FIGURE 6. **Association and dissociation of fission yeast capping protein (*Sp*CP) on filament barbed ends analyzed by an HMM method.** Conditions used were as follows: buffers as in Fig. 1. *A,* time series of fluorescence micrographs of actin filaments growing in the presence 1 μM (20% labeled) Mg-ATP-actin and 64 nM *Sp*CP (added at 12 min, *plus symbols in each frame*). Filament barbed ends alternated between growing at a constant rate (*open arrowheads*) and halting (*closed arrowheads*). Representative filaments marked *a* and *b* are highlighted in *B* and *C*. Numbers (*min:s*) indicate frame times. *Scale bar* is 10 μm. *B,* time course of the change in length of representative filaments. The *dashed line* indicates the step increase in *Mm*CP. *C,* derivative of length *versus* time data from *B* showing instantaneous growth rates of representative filaments. The *dashed line* indicates the step increase in *Mm*CP. Filaments either grew uniformly at 7.4 subunits·s^{-1} (uncapped state) or zero subunits·s^{-1} (capped state). Baum-Welch estimations (*bold lines*) were used to "idealize" the capped (down) or uncapped (up) state of a filament at each time point. *D,* dependence of the apparent rate (sum of association and dissociation rates as described under "Experimental Procedures") on the concentration of *Sp*CP. We used MIL optimizations to estimate an apparent equilibrium rate, k_{app}, for a range of *Sp*CP concentrations. Linear regression (*bold line*) provided an association rate constant of 1.1×10^5 M^{-1} s^{-1}, a dissociation rate constant of 3.1×10^{-3} s^{-1}, and a K_d of 29 nM. *E* and *F,* effect of PPIs on the association (*E*) and dissociation (*F*) rate constants for *Sp*CP binding to filament barbed ends. Both the association and dissociation rate constants were estimated at a single *Sp*CP concentration by the HMM method from movies of filaments growing intermittently in 0.5 μM (50% labeled) Mg-ATP actin, 20 nM *Sp*CP (concentration adjusted for active fraction of frozen stock), and 25 μM of the indicated phosphoinositide or buffer. Values shown are the mean and S.D. of three experiments (average of 199 total events) per condition. The mean association and dissociation rate constants obtained in *D* are shown for comparison in *E* and *F* (*No PI, dark bars*).

We also tested the uncapping hypothesis by microscopic observations of filaments stabilized with phalloidin. We elongated unlabeled filament seeds with a high mole fraction of OG-actin followed by capping by *Mm*CP. We diluted these seeds into polymerization buffer with a low mole fraction of OG-actin to learn if any barbed end elongated. After 5 min we stabilized and labeled the filaments with rhodamine-phalloidin. Uncapped filaments (Fig. 5*A*) had a characteristic staining pattern of red pointed ends, bright green middles, and dim green barbed ends, whereas capped filaments (Fig. 5*B*) had red pointed ends and bright green barbed ends. Using these criteria, we counted the number of capped and uncapped filament in each condition and ignored broken filaments. In control experiments without capping protein, 88 ± 5% of filaments had an uncapped staining pattern. With capping protein, the fraction of uncapped filaments dropped to 6 ± 3%. At concentrations of 20 μM, neither PI (10 ± 8% uncapped; data not shown), $PI(3,4)P_2$ (11 ± 4% uncapped; data not shown), $PI(4,5)P_2$ (15 ± 4% uncapped; Fig. 5*C*), nor $PI(3,4,5)P_3$ (14 ± 5% uncapped; data not shown) uncapped the filaments during 5 min of incubation (Fig. 5*D*). Thus, the increase in free barbed ends seen in bulk uncapping experiments is unlikely to be due to uncapping.

Interactions of Fission Yeast Capping Protein with Actin Filament Barbed Ends—Filaments growing from skeletal muscle Mg-ATP-actin monomers in the presence of fission yeast capping protein fluctuated between phases of steady elongation and pauses (Fig. 6, *A* and *B*). The pauses presumably represent

TABLE 3
***S. pombe* capping protein rate and equilibrium constants**

Experiment	k_+ Markov	k_- Markov	k_- direct[a]	K_d[b]	K_d[c]
	$\times 10^5\ M^{-1}\cdot s^{-1}$	$\times 10^{-3}\ s^{-1}$	$\times 10^{-3}\ s^{-1}$	nM	nM
Apparent rate *versus* concentration	1.1 ± 0.2	3.1 ± 3.1	5.7 ± 0.1	29	52
Average with PI buffer	0.9 ± 0.3	5.1 ± 2.1	3.8 ± 0.4	60	45
with 25 μM PI	1.2 ± 0.1	5.7 ± 0.5	4.4 ± 0.2	49	38
with 25 μM $PI(3,4)P_2$	0.9 ± 0.3	4.8 ± 0.8	4.1 ± 1.0	51	44
with 25 μM $PI(4,5)P_2$	0.9 ± 0.1	5.7 ± 2.0	2.9 ± 0.1	64	33
with 25 μM $PI(3,4,5)P_3$	1.0 ± 0.4	5.8 ± 2.1	2.6 ± 1.2	56	26

[a] Direct dissociation rate experiment is shown for the slow component of the double exponential fit.
[b] Average Markov dissociation rate/average Markov association rate is given.
[c] Direct dissociation rate/average Markov association rate is given.

capping events, which end by dissociation of *Sp*CP from barbed ends followed by elongation. Short pauses are difficult to detect by time lapse TIRF microscopy, so we could not measure *Sp*CP association directly. Rather, because capping protein binding to filaments is a stochastic Markov process, we used growth traces of individual filaments and hidden Markov modeling (HMM) to estimate the "hidden" capped or uncapped state of each filament at each time point along with the association and dissociation rates of *Sp*CP at filament barbed ends.

We tracked the lengths of 10–15 filaments per experiment over time to obtain individual growth curves (Fig. 6*B*) and their derivatives. Growth rates were linear, but individual length measurements varied by 200–400 subunits (S.E.) from the expected value because of filament motion. We took the derivative of the growth data for each filament to obtain the instantaneous growth rate at each frame (Fig. 6*C*). Although growth rates were uniform throughout the field for the uncapped state and essentially zero during the capped state (Fig. 6, *B* and *C*), noise in the rate data hindered manual assignment of state transitions. We therefore used the Baum-Welch algorithm (38) to assign capped or uncapped state to rate traces based on the local amplitude and noise of each segment. We combined sections of obvious linear growth or capping from four filaments to obtain the mean (amplitude) and standard deviation (noise) of growth rates for each experiment. The Baum-Welch interval detection algorithm used these values, along with an initial estimate of the association and dissociation rate constants to estimate the hidden capping state of each filament (Fig. 6*C*, *bold lines*). A maximum interval likelihood (MIL) algorithm then used the fractional occupancy of each state and frequencies of transitions from capped to uncapped or vice versa to estimate the rates of transition between these two states. Using these new rate constants, we reapplied the Baum-Welch interval detection to refine the state occupancies followed by the MIL algorithm to refine rate constants. We repeated this process until the rate constants stabilized. The apparent rate estimated by HMM (Fig. 6*D*) was proportional to the concentration of *Sp*CP, giving an association rate constant of 0.11 $\mu M^{-1}\ s^{-1}$ and a dissociation rate constant of $3.1\times10^{-3}\ s^{-1}$ for a binding affinity of 29 nM.

To measure *Sp*CP dissociation rates directly, we grew Mg-ATP-actin seeds in flow cells, equilibrated them for 5 min with *Sp*CP, and removed capping protein by washing with higher fraction-labeled Mg-ATP actin. We estimated *Sp*CP dissociation times from the resumption of filament growth as in Fig. 2 (not shown) and observed a single exponential dissociation rate constant of $5.7 \pm 0.1 \times10^{-3}\ s^{-1}$ (half-time of 2 min).

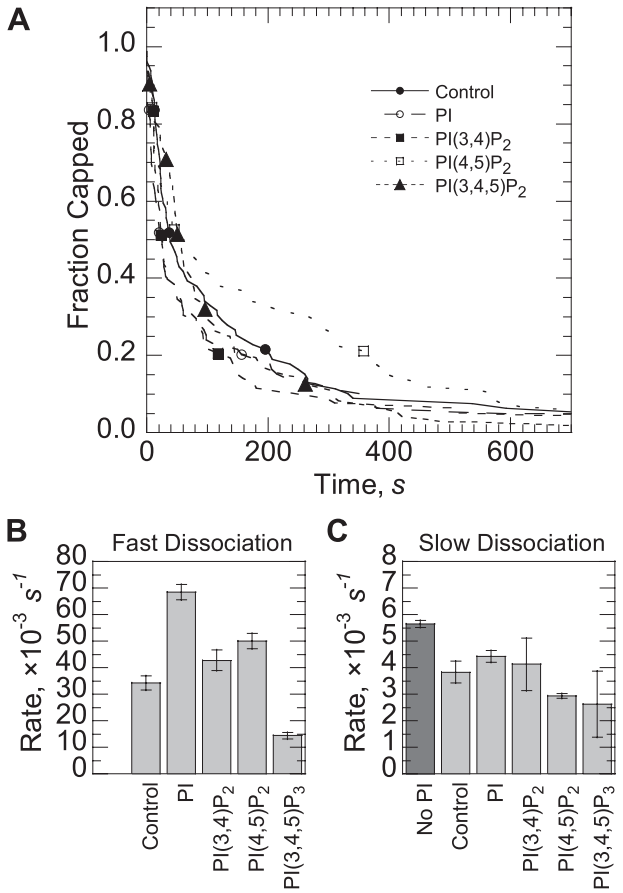

FIGURE 7. **Dissociation of fission yeast capping protein from actin filament barbed ends.** Conditions used were as follows: buffers as in Fig. 1. *A,* time course of the uncapping of actin filament barbed ends. Actin filament seeds were grown in flow chambers from 1 μM (25% labeled) Mg-ATP and incubated with 40 nM *Sp*CP for 5 min. Uncapping was initiated by exchanging the chamber buffer with 1 μM (50% labeled) Mg-ATP-actin alone or with 25 μM of PPI. These data come from three experiments with an average of 75 dissociation events per condition. These data were best fit by the sum of two exponentials (not shown) as explained in the text. *B,* fast exponential dissociation rates from *A*. *C,* slow exponential dissociation rates from *A*. Values represent means and S.E. of estimation of the fit. The single exponential rate constant from a separate experiment (*No PI, dark bar*) is shown for comparison.

Unlike murine capping protein, 25 μM phosphoinositides did not significantly affect the rate of association of 20 nM *Sp*CP with actin filaments (Fig. 6*E*; Table 3). We observed the effects of phosphoinositides on *Sp*CP dissociation by equilibrating filaments with *Sp*CP and then washing *Sp*CP out of the reaction buffer with higher fraction-labeled actin and 25 μM phosphoinositide or buffer. The time course of the initiation of regrowth (Fig. 7*A*) was best fit by the sum of two exponentials as follows:

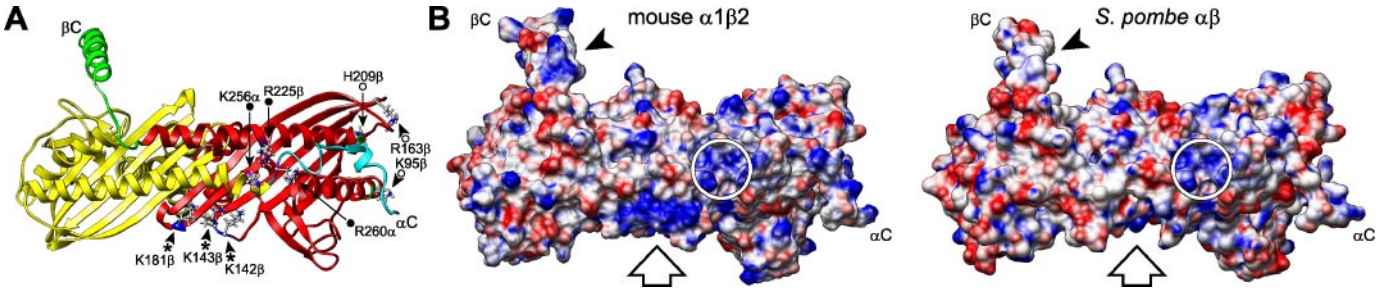

FIGURE 8. **Homology models of *Mm*CP and *Sp*CP reveal a potential PPI-binding site.** Homology models based on the crystal structure of chicken CP (3) showing the actin-binding surface. *A,* ribbon diagram of the homology model of mouse CP with a *yellow* α1 subunit and a *red* β2 subunit. The *arrows* mark potential PPI-binding sites: ○, residues flanking two nitrate-binding sites proposed by Yamashita *et al.* (3) from their crystal structure; ●, site found by Kim *et al.* (13); ▶, large positively charged site missing in *S. pombe* and proposed by Smith *et al.* (39). The carboxyl-terminal α- (*cyan*) and β-tentacles (*green*) are highlighted along with proposed PPI-binding residues. *B,* surface representations of mouse (*left*) and *S. pombe* (*right*) CP homology models. Surfaces are colored for iso-potential values of +15 (*blue*), 0 (*white*), and −15 (*red*) k_BT/e_c. *Arrows* indicate regions of positive charge that are present on the actin-binding surface (*large arrow*) and β-tentacle (*arrowhead*) of mouse CP but absent in *pombe* CP. *Large circles* indicate the PIP_2-binding site found by Kim *et al.*

a fast dissociation half-life of 10–50 s with an amplitude of 0.6 (Fig. 7*B*), and a slow dissociation half-life of 2–4 min with an amplitude of 0.4 (Fig. 7*C*). Our analysis assumed that every filament was capped at the start of the experiment, but *Sp*CP rapidly associated and dissociated from filaments. The fast dissociation therefore likely represents filaments that were not capped during the final buffer exchange. As we observed a slow single exponential dissociation in other experiments (not shown), the slow dissociation likely represents the true dissociation rate constant for *Sp*CP in the presence of phosphoinositides. Like murine capping protein, phosphoinositides did not significantly affect fission yeast capping protein dissociation when measured directly (Fig. 7*C*) or via HMM estimation (Fig. 6*F* and Table 3).

Homology Models to Identify Potential PPI-binding Sites in CP—The lack of effect of PPIs on *Schizosaccharomyces pombe* CP offers an experiment of nature to provide clues regarding PPI-binding sites on other CPs. We constructed homology models of capping proteins from several species based on the crystal structure of chicken CP (3) (supplemental Fig. 1). Vertebrate, insect, and plant CPs have a large area of positive potential on the β subunit mushroom "head" (Fig. 8*A*, Lys-142, Lys-143, and Lys-181) that is absent in fission yeast (Fig. 8*B*, *large arrows*) and reduced in budding yeast CPs (data not shown). This large basic patch was proposed as a potential PPI-binding site based on hydrophobic scanning of the CP sequence (39) and lies on the surface that interacts with the barbed end of an actin filament (3, 34). It is thus a strong candidate to contribute to PPI binding. This basic patch is adjacent to but distinct from a cluster of basic residues in the α-tentacle hinge region of many CPs, including fission yeast CP. Mutation of three of the basic residues in the hinge region reduce the affinity of chicken CP for PIP_2 about 4-fold (13).

DISCUSSION

By directly observing capping and uncapping of actin filaments with TIRF microscopy, we obtained association and dissociation rate constants for mouse CP very similar to those previously obtained through bulk polymerization assays (4). These previous measurements fitted polymerization curves of bulk samples to a simple model of capping without contributions from filament nucleation, breakage, annealing, and pointed end growth, so these side reactions must be negligible in carefully executed bulk capping experiments.

We also agree with Schafer *et al.* (4) that PPIs appear to uncap filaments in a bulk polymerization assay. On the other hand, PPIs did not uncap actin filaments in either of our microscopy assays. Control experiments provided evidence for an hypothesis to reconcile these apparently contradictory observations. We found that mixing can break long capped filaments in bulk samples, thus exposing new barbed ends. In the presence of CP, these barbed ends are rapidly recapped unless PPIs sequester the capping protein. This gives the appearance of uncapping by PPIs. Filament breakage and annealing were not considered in the previous bulk uncapping experiments (4), perhaps because they utilized spectrin-actin seeds with filaments of only 13–14 subunits (40). However, we calculate from the actin polymer concentration and exponential capping rate that half of the filaments were at least 4.1 μm long, 25% were at least 6.2 μm long, and 2% of filaments were uncapped and 16.9 μm long at the time that Schafer *et al.* (4) added PIP_2 in their uncapping experiment. Filaments this long were subjected to breakage in our control experiments.

Any bulk assay designed to test for uncapping activity must distinguish filament breakage combined with CP sequestration from noncompetitive removal of CP from filament ends. Similar assays using spectrin-actin seeds led to the conclusion that Ena/VASP (5, 7) and CARMIL (8) compete capping protein from filaments, so the uncapping activities of these important CP inhibitors should be verified at a single filament level.

We confirmed earlier observations that $PI(3,4)P_2$ and $PI(4,5)P_2$ inhibit capping *in vitro* (4, 10) at the single filament level, but unlike Schafer (4), we also found a substantial inhibition of capping by $PI(3,4,5)P_3$. Assuming a bimolecular reaction of *Mm*CP with PPI and that only free *Mm*CP participates in capping, the dissociation equilibrium constants for *Mm*CP binding PIP_2 and PIP_3 are in the range of 5–10 μM in 1 mM $MgCl_2$ and about 10-fold lower in 0.1 mM $MgCl_2$.

Kim *et al.* (13) also investigated uncapping by PPIs using TIRF microscopy. They introduced capped filaments into flow cells, then flowed PIP_2 and fresh actin into the chambers, and counted the fraction of growing filaments at 5-min intervals. With 50 μM PIP_2, twice the concentration that appeared to

uncap filaments rapidly in their bulk assay, only 10% of filaments were growing after 40 min, the half-time for CP dissociation. Even in the absence of PIP_2, only 12% of filaments were growing 60 min after CP washout. Based on their estimated dissociation rate constant of 5.7×10^{-4} s^{-1}, 87% of filaments should have been uncapped within 60 min. This low fraction of growing filaments might be explained if a substantial amount of free CP remained in the chamber to recap barbed ends. Apparent uncapping half-times faster than the natural CP dissociation half-time of 40 min were only seen at 150–500 μM PIP_2. As filament breakage because of Brownian motion of filaments and evaporative flow are problematic in TIRF assays (for example, see filaments *b–d* in Fig. 1*B*), the life history of every filament must be observed to rule out growth because of filament breakage rather than uncapping. Although we cannot rule out allosteric uncapping at very high concentrations of PIP_2, another explanation is that PIP_2 sequestered the remaining free CP and prevented re-capping of uncapped or broken filaments in their assay. Alternatively, insufficient slide blocking after the *N*-ethylmaleimide myosin-II wash step can lead to an overly adherent surface that could block either filament growth or CP dissociation because of nonspecific binding of capped or uncapped filament ends to the glass surface. High concentrations of negatively charged lipids could act as an efficient slide blocking agent, allowing barbed ends to grow as they broke or uncapped. As filaments were capped prior to their introduction into flow cells in the study of Kim *et al.* (13), only uncapping would be affected by nonspecific adherence. In either case, ensuring that TIRF microscopy can accurately measure the same CP dissociation rates seen in bulk assays without PPIs is essential for determining the dissociation rates in the presence of PPIs.

Uncapping is a possible mechanism to explain how PPIs stimulate the creation of actin filament barbed ends in cells and permeabilized cells (9, 41). However, given our evidence that PPIs sequester CP but do not uncap filaments, PPIs are more likely to generate barbed ends by acting on activators of Arp2/3 complex or other mechanisms. These alternatives are consistent with the observation that stimulation of *Dictyostelium* with cAMP generates free barbed ends while increasing, rather than decreasing, CP association with the actin cytoskeleton (11). Similarly, mechanisms other than uncapping must be considered to explain the strong bias in the orientation of barbed ends toward the leading edge of motile cells (12).

Gelsolin can simultaneously sever and cap actin filaments (42), but severing activity has never been reported for CP. Filaments can break spontaneously while being observed with TIRF illumination. Without CP the new barbed end grows. In the presence of CP some broken filaments grew (Fig. 1*B*, filament *d*) but others did not (Fig. 1*B*, filament *b*). Thus capping protein may have a low level of severing activity, although these events may be because of spontaneous breakage followed by rapid capping.

Observations on Fission Yeast Capping Protein—S. pombe CP has the most divergent biochemical properties among the various CPs studied to date. *Sp*CP binds the barbed end of vertebrate actin filaments 30–50 times slower and dissociates 10 times faster than mouse CP and is the only characterized CP that is not inhibited by PPIs. These differences provide a window to examine the structural basis of these binding reactions. *S. pombe* CP has a greater overall negative charge (−26.5) at pH 7.0 than mouse CP (−13.2), so electrostatic repulsion from negatively charged actin and PPIs may contribute to the lower affinities. More importantly, both the positive charge along the actin-binding (43) surface (Fig. 8*B*, *large arrow*) and on the flexible, actin-binding β-tentacle (Fig. 8*B*, *arrowhead*) are substantially greater on *Mm*CP than *Sp*CP.

The larger of these positive patches is also an attractive potential PPI-binding site. First, it is one of the amphipathic sites predicted as a potential PIP_2-binding site by a theoretical analysis of CP structure (39). Second, the absence of this basic patch in *S. pombe* CP can explain the lack of PPI binding. Third, binding of PIP_2 or PIP_3 to this basic patch would sterically hinder actin binding. Fourth, binding to the barbed end of an actin filament would preclude binding of PIP_2 or PIP_3 micelles to this site, accounting for their inability to dissociate *Mm*CP from actin filaments.

Mutational analysis of mouse CP (13) identified an inhibitory PIP_2-binding site flanked by three residues, α1(Lys-256), α1(Arg-260), and β1(Arg-225), near the α-COOH terminus. Although triple mutation of all three residues reduced the affinity of CP for PIP_2 5-fold in a tryptophan fluorescence assay and 60-fold in an activity-based assay, the affinity of the CP triple mutant for filament barbed ends was reduced 450-fold, complicating any interpretation of competition between PIP_2 and barbed ends for CP at this site. Furthermore, these sites are well conserved in fission yeast and are less likely to explain the lack of PPI binding seen here. Further mutational analysis of the large basic patch proposed here and by Smith *et al.* (39) would be instructive.

Yamashita *et al.* (3) proposed another candidate PPI-binding site where residues His-209, Arg-163, and Lys-95 of the β subunit bind two nitrates (Fig. 8*B*) in the crystal structure of chicken CP. Given the location of these residues below the α-tentacle, away from the actin-binding region (43), PPI binding at this site would have to act allosterically to affect CP activity. Furthermore, two of these three residues are also present in both yeast species and consequently cannot account for the lack of PPI binding in *S. pombe* CP. Although mutational analysis of one of these residues, β1(Lys-95), failed to show any effect on PIP_2 binding (13), the nitrate-binding site cannot yet be ruled out as a PPI-binding site.

Little is known about the links between phosphatidylinositol signaling and the actin cytoskeleton in yeast. Both fission and budding yeast contain functional PI (4)P 5-kinases (*its3* in fission yeast and *mss4* in budding yeast). At the restrictive temperature, temperature-sensitive mutations of these PI (4)P 5-kinases lead to reduced actin cables and disruption in actin patch polarity but not patch number. In contrast, cytokinetic actin rings are normal in *its3-1* mutations at the restrictive temperature. Given that neither PIP_2 nor PIP_3 affects the interaction of *Sp*CP with actin and that PIP_2 reduction alters the localization but not the maturation of actin patches, it is likely that PIP_2 acts upstream rather than directly on CP in yeast.

The association rate constant for *Sp*CP fits well with the time course of actin patch formation. Actin patches assemble and disassemble within 20 s (44) and contain about one CP dimer

for every two Arp2/3 complexes (45). Thus, about half of all barbed ends are capped at any point in time. With a cytoplasmic concentration of 1.2 μM (45) and an association rate constant of 0.04 μM^{-1} s^{-1}, the half-time for capping would be 14 s. This is a bit too slow to cap all of the filaments during the 10-s growth phase, so macromolecular crowding may speed up the reaction in the cell. The 2-min half-time for dissociation of *Sp*CP from filaments is long enough to protect barbed ends from further polymerization during the 10-s disassembly phase and some other mechanism must account for the rapid depolymerization.

REFERENCES

1. Svitkina, T. M., and Borisy, G. G. (1999) *J. Cell Biol.* **145,** 1009–1026
2. Mullins, R. D., Heuser, J. A., and Pollard, T. D. (1998) *Proc. Natl. Acad. Sci. U. S. A.* **95,** 6181–6186
3. Yamashita, A., Maeda, K., and Maeda, Y. (2003) *EMBO J.* **22,** 1529–1538
4. Schafer, D. A., Jennings, P. B., and Cooper, J. A. (1996) *J. Cell Biol.* **135,** 169–179
5. Bear, J. E., Svitkina, T. M., Krause, M., Schafer, D. A., Loureiro, J. J., Strasser, G. A., Maly, I. V., Chaga, O. Y., Cooper, J. A., Borisy, G. G., and Gertler, F. B. (2002) *Cell* **109,** 509–521
6. Svitkina, T. M., Bulanova, E. A., Chaga, O. Y., Vignjevic, D. M., Kojima, S., Vasiliev, J. M., and Borisy, G. G. (2003) *J. Cell Biol.* **160,** 409–421
7. Barzik, M., Kotova, T. I., Higgs, H. N., Hazelwood, L., Hanein, D., Gertler, F. B., and Schafer, D. A. (2005) *J. Biol. Chem.* **280,** 28653–28662
8. Uruno, T., Remmert, K., and Hammer, J. A. (2006) *J. Biol. Chem.* **281,** 10635–10650
9. Hartwig, J. H., Bokoch, G. M., Carpenter, C. L., Janmey, P. A., Taylor, L. A., Toker, A., and Stossel, T. P. (1995) *Cell* **82,** 643–653
10. Heiss, S. G., and Cooper, J. A. (1991) *Biochemistry* **30,** 8753–8758
11. Eddy, R. J., Han, J., and Condeelis, J. S. (1997) *J. Cell Biol.* **139,** 1243–1253
12. Maly, I. V., and Borisy, G. G. (2001) *Proc. Natl. Acad. Sci. U. S. A.* **98,** 11324–11329
13. Kim, K., McCully, M. E., Bhattacharya, N., Butler, B., Sept, D., and Cooper, J. A. (2007) *J. Biol. Chem.* **282,** 5871–5879
14. Amatruda, J. F., and Cooper, J. A. (1992) *J. Cell Biol.* **117,** 1067–1076
15. Kuhn, J. R., and Pollard, T. D. (2005) *Biophys. J.* **88,** 1387–1402
16. Pollard, T. D. (1984) *J. Cell Biol.* **99,** 769–777
17. Palmgren, S., Ojala, P. J., Wear, M. A., Cooper, J. A., and Lappalainen, P. (2001) *J. Cell Biol.* **155,** 251–260
18. Kovar, D. R., Wu, J. Q., and Pollard, T. D. (2005) *Mol. Biol. Cell* **16,** 2313–2324
19. Kielley, W. W., and Harrington, W. F. (1960) *Biochim. Biophys. Acta* **41,** 401–421
20. Amann, K. J., and Pollard, T. D. (2001) *Proc. Natl. Acad. Sci. U. S. A.* **98,** 15009–15013
21. Houk, T. W., Jr., and Ue, K. (1974) *Anal. Biochem.* **62,** 66–74
22. Margossian, S. S., and Lowey, S. (1982) *Methods Enzymol.* **85,** 55–71
23. Kouyama, T., and Mihashi, K. (1981) *Eur. J. Biochem.* **114,** 33–38
24. Pollard, T. D. (1986) *J. Cell Biol.* **103,** 2747–2754
25. Sabanayagam, C. R., Smith, C. L., and Cantor, C. R. (2000) *Nucleic Acids Res.* **28,** E33–E36
26. Huxley, H. E., and Brown, W. (1967) *J. Mol. Biol.* **30,** 383–434
27. Savitzky, A., and Golay, M. J. E. (1964) *Anal. Chem.* **36,** 1627–1639
28. Qin, F., Auerbach, A., and Sachs, F. (1996) *Biophys. J.* **70,** 264–280
29. Qin, F. (2004) *Biophys. J.* **86,** 1488–1501
30. Edgar, R. C. (2004) *Nucleic Acids Res.* **32,** 1792–1797
31. Schwede, T., Kopp, J., Guex, N., and Peitsch, M. C. (2003) *Nucleic Acids Res.* **31,** 3381–3385
32. Baker, N. A., Sept, D., Joseph, S., Holst, M. J., and McCammon, J. A. (2001) *Proc. Natl. Acad. Sci. U. S. A.* **98,** 10037–10041
33. Pettersen, E. F., Goddard, T. D., Huang, C. C., Couch, G. S., Greenblatt, D. M., Meng, E. C., and Ferrin, T. E. (2004) *J. Comput. Chem.* **25,** 1605–1612
34. Wear, M. A., Yamashita, A., Kim, K., Maeda, Y., and Cooper, J. A. (2003) *Curr. Biol.* **13,** 1531–1537
35. Janmey, P. A., and Stossel, T. P. (1989) *J. Biol. Chem.* **264,** 4825–4831
36. Schafer, D. A., Korshunova, Y. O., Schroer, T. A., and Cooper, J. A. (1994) *J. Cell Biol.* **127,** 453–465
37. Janmey, P. A., Hvidt, S., Kas, J., Lerche, D., Maggs, A., Sackmann, E., Schliwa, M., and Stossel, T. P. (1994) *J. Biol. Chem.* **269,** 2503–2513
38. Baum, L. E., Petrie, T., Soules, G., and Weiss, N. (1970) *Ann. Math. Statist.* **41,** 164–171
39. Smith, J., Diez, G., Klemm, A. H., Schewkunow, V., and Goldmann, W. H. (2006) *Theor. Biol. Med. Model.* **3,** 30–36
40. Byers, T. J., and Branton, D. (1985) *Proc. Natl. Acad. Sci. U. S. A.* **82,** 6153–6157
41. Tolias, K. F., Hartwig, J. H., Ishihara, H., Shibasaki, Y., Cantley, L. C., and Carpenter, C. L. (2000) *Curr. Biol.* **10,** 153–156
42. Harris, H. E., and Weeds, A. G. (1984) *FEBS Lett.* **177,** 184–188
43. Narita, A., Takeda, S., Yamashita, A., and Maeda, Y. (2006) *EMBO J.* **25,** 5626–5633
44. Sirotkin, V., Beltzner, C. C., Marchand, J. B., and Pollard, T. D. (2005) *J. Cell Biol.* **170,** 637–648
45. Wu, J. Q., and Pollard, T. D. (2005) *Science* **310,** 310–314